The Spine Journal 24 (2024) 2191–2203

Basic Science

Evaluating the biomechanical effects of pedicle subtraction osteotomy at different lumbar levels: a finite element investigation

Niloufar Shekouhi, MS[a], Sudharshan Tripathi, MS[a], Alekos Theologis, MD[b], Muzammil Mumtaz, PhD[a], Hassan Serhan, PhD[a], Robert McGuire, MD[c], Vijay K. Goel, PhD[a,*], Joseph M. Zavatsky, MD[d]

[a] *Engineering Center for Orthopedic Research Excellence (E-CORE), Departments of Bioengineering and Orthopaedic Surgery, University of Toledo, Toledo, OH, USA*
[b] *Department of Orthopedic Surgery, University of California- San Francisco (UCSF), San Francisco, CA, USA*
[c] *Department of Orthopedic Surgery, University of Mississippi Medical Center, Jackson, MS, USA*
[d] *Spine & Scoliosis Specialists, Tampa, FL, USA*

Received 12 February 2024; revised 3 July 2024; accepted 27 July 2024

Abstract

BACKGROUND: Pedicle subtraction osteotomy (PSO) is effective for correcting spinal malalignment but is associated with high complication rates. The biomechanical effect of different PSO levels remains unclear, and no finite element (FE) analysis has compared L2-, L3-, L4-, and L5-PSOs.
PURPOSE: To assess the effects of PSO level on the spine's global range of motion, stresses on posterior instrumentation, load sharing with the anterior column, and proximal junctional stresses.
STUDY DESIGN: A computational biomechanical analysis.
METHODS: A validated 3D spinopelvic FE model (T10-Pelvis) was used to perform PSOs at L2, L3, L4 and L5. Each model was instrumented with a 4-rod configuration (primary rods + *in-line* satellite rods) from T11-Pelvis. Simulation included a 2-step analysis; (1) applying 300 N to thoracic, 400 N to lumbar, and 400 N to sacrum, and (2) applying a 7.5 Nm moment to the top endplate of the T10 vertebral body. Acetabulum surfaces were fixed in all degrees of freedom. The range of motion, spinopelvic parameters (lumbar lordosis [LL], sacral slope [SS], pelvic incidence [PI], and pelvic tilt [PT]), PSO force, and von Mises stresses were measured. All models were compared with the L3-PSO model and percentage differences were captured.
RESULTS: Compared to the intact alignment: LL increased by 48%, 45%, 59%, and 56% in the L2-, L3-, L4-, and L5-PSO models; SS increased by 25%, 15%, and 11% while PT decreased by 76%, 53%, and 45% in L2-, L3-, and L4-PSOs (SS and PT approximated intact model in L5-PSO); Lumbar osteotomy did not affect the PI. Compared to L3-PSO: L2-, L4-, and L5-PSOs showed up to 32%, 34%, and 34% lower global ROM. The least T10-T11 ROM was observed in L5-PSO. The left and right SIJ ROM were approximately similar in each model. Amongst all, the L5-PSO model showed the least ROM at the SIJ. Compared to L3-PSO, the L2-, L4-, and L5-PSO models showed up to 67%, 61%, and 78% reduced stresses at the UIV, respectively. Minimum stress at UIV+ was observed in the L3-PSO

FDA device/drug status: Not applicable.

Author disclosures: ***NS:*** Nothing to disclose. ***ST:*** Nothing to disclose. ***AT:*** Royalties: Alphatec (E); Consulting: DePuy Spine (D), Ulrich Medical USA (E), Surgalign (E), Icotec (C), Carbofix (B), Restor3D (B), Stryker/K2M (C); Trips/Travel: AO Spine (B); Research Support (Investigator Salary, Staff/Materials): NIH/NSF (E, Paid directly to institution/employer). ***MM:*** Nothing to disclose. ***HS:*** Nothing to disclose. ***RM:*** Trips/Travel: AO Foundation (Amount not disclosed); Board of Directors: AO Foundation (Amount not disclosed). ***VKG:*** Grant: NSF CDMI (C, Paid directly to institution/employer); Royalties: Globus Medical (Amount not disclosed); Stock Ownership: Spinal Balance (Amount not disclosed), OsteoNovus (Amount not disclosed), Intellisenze (Amount not disclosed); Grants: NSF (Amount not disclosed). ***JMZ:*** Royalties: Zimmer Biomet (B).

*Corresponding author. Engineering Center for Orthopaedic Research Excellence (E-CORE), Department of Bioengineering and Orthopaedic Surgery, Colleges of Engineering and Medicine, University of Toledo, Univ of Toledo, 2801 West Bancroft Street, MS 303, NI Hall, Room 5046, Toledo, OH 43606, USA.

E-mail address: Vijay.Goel@utoledo.edu (V.K. Goel).

https://doi.org/10.1016/j.spinee.2024.07.005

model. The L2-and L3-PSOs showed the maximum PSO force. The L5-PSO model showed the lowest stresses on the primary rods in all motions.

CONCLUSION: Our FE investigation indicates that L5-PSO results in the greatest lumbar lordosis and lowest global, SIJ, and T10-T11 ROMs and stresses on the primary rods, suggesting potential mechanical benefits in reducing the risk of rod breakage. However, L4- and L5-PSOs led to the least force across the osteotomy site, which may increase the risk of pseudarthrosis. These findings provide biomechanical insights that may inform surgical planning, though further clinical investigation is essential to determine the optimal PSO level and validate these results.

CLINICAL SIGNIFICANCE: Understanding the biomechanical impact of PSO level is crucial for optimizing surgical outcomes and minimizing the risks of postoperative complications.

Keywords: Finite element analysis; Pedicle subtraction osteotomy; Rod fracture; Pseudarthrosis; Proximal junctional kyphosis; Proximal junctional stresses

Introduction

Restoration of lumbopelvic harmony, pelvic tilt, and global sagittal balance are fundamental goals of sagittal spinal deformity correction. One of the most commonly used surgical strategies to restore sagittal balance is the pedicle subtraction osteotomy (PSO). In a PSO, the posterior elements, pedicles, and a V-shaped wedge of the vertebral body through the pedicles are resected, and the osteotomy is closed and stabilized by means of posterior fixation. PSOs are commonly performed at the L3 vertebra. However, according to Roussouly et al [1,2], the inferior segments (between L4 and S1) have a higher influence on lumbar lordosis and osteotomies in these regions can lead to a greater sagittal correction.

Although the PSO is a powerful surgical technique, it is associated with high rates of complications (proximal junctional kyphosis (PJK), implant failure, and pseudarthrosis [3–12]) and hence still remains challenging. PJK is a common complication following long segmental spinal fusion with reported rates ranging from 17% to 61.7% [13–16]. PJK is defined as a proximal junctional sagittal Cobb angle (between the upper instrumented vertebra (UIV) and 2 super-adjacent segments) of 10° or higher [14]. In severe cases, PJK can result from ligamentous disruption or fracture, which may require revision surgery. Excessive curvature correction [17–20], abnormal preoperative sagittal parameters [17,18,21–24], lumbar and sacral fusions [22,23,25–27], and the number of instrumented levels [18,19,25,28] are reported as risk factors for PJK [14].

Previous PSO investigation has primarily focused on resultant changes in global sagittal alignment as well as relative sagittal lumbopelvic corrective potentials based on PSO level [29]. However, as more evidence highlights the importance of restoring relative lumbar lordosis based on pelvic and spinal morphologies [30], in relation to mechanical complications, including PJK [31], an understanding of the effect of PSO level on proximal junctional stresses and load sharing with the anterior column is critically important to minimize the incidence of PJK and pseudarthrosis. The purpose of the current study was to assess the effect of PSO level on the spine's global range of motion, stresses on posterior instrumentation, load sharing with the anterior column, and proximal junctional stresses.

Material and methods

In this study, a previously validated osseoligamentous 3-dimensional spinopelvic model (T10-pelvis) was used to develop 30° PSOs at different vertebral levels at L2, L3, L4, and L5 [32,33]. The intact model was reconstructed from computed tomography (CT) scans of a human spine using MIMICS (Materialize Inc., Leuven, Belgium) software. IAFE-MESH (University of Iowa, Iowa) and HyperMesh (Altair Engineering, Michigan, USA) were used to create hexahedral elements (C3D8) of the vertebrae and tetrahedral elements (C3D4) of the pelvis. The meshed components were assembled in Abaqus 6.14 (DassaultSystemes, Simile Inc., Providence, RI, USA). The spinal and sacroiliac ligaments were modeled using truss elements. In the vertebral body, a layer of 0.5 mm cortical bone was simulated to surround the cancellous bone.

The intervertebral discs were composed of annulus fibrosis and nucleus pulposus. The annulus fibrosis was simulated using a solid ground substance (C3D8 elements) reinforced with rebar elements (embedded with 30 angles). The nucleus pulposus was modeled using C3D8 elements with a hyper-elastic Mooney-Rivlin formulation. The sacroiliac joint was modeled using soft contact with exponential behavior. Material properties were adapted from literature and assigned to each component (Table 1) [33].

An extensive explanation of the L3-PSO model development can be found in the literature [32,33]. A similar approach was utilized to develop 30° PSOs at L2, L3, L4, and L5 levels (Fig. 1). In all models, the anterior section was tied, and a surface-to-surface interaction (friction=0.46) was defined between the 2 resected segments at the posterior site.

Spinopelvic parameters

For intact and each PSO model, the following spinopelvic parameters were measured [34]:

Table 1
Material properties used in model development adapted from literature [32,33]

Components	Element formulation	Young's modulus (MPa)/Poisson's ratio
Vertebral cortical bone	Isotropic, elastic hex elements (C3D8)	12,000/0.3
Vertebral cancellous bone	Isotropic, elastic hex elements (C3D8)	100/0.2
Pelvic cortical bone	Isotropic, elastic hex elements (C3D8)	17,000/0.3
Pelvic cancellous bone	Isotropic, elastic hex elements (C3D8)	10/0.2
Annulus (ground)	Neo-Hookean, hex elements (C3D8)	C10=0.348, D1=0.3
Annulus (fiber)	Rebar	357–550
Nucleus	Mooney Rivlin hex elements (C3D8H)	C1=0.12, C2=0.03, D1=0.0005
Apophyseal joints	Nonlinear soft contact, GAPUNI elements	-
Sacroiliac joints	Nonlinear soft contact	-
Ligaments	Hypo-elastic, tension only, Truss elements (T3D2)	Nonlinear stress–strain curves
Ti6Al4V pedicle screws	Isotropic, tetrahedron elements (C3D4)	11,500/0.3
CoCr rods	Isotropic, tetrahedron elements (C3D4)	241,000/0.3

- L1-S1 lordosis (LL): The angle between the superior endplates of L1 and S1.
- L4-S1 lordosis: The angle between the superior endplates of L4 and S1.
- Sacral Slope (SS): The angle between the superior endplate of S1 with the horizontal line.
- Pelvic Incidence (PI): The morphological variable which is defined as the angle between the sacral perpendicular line with a line connecting the center of the femoral head and the center of the sacrum.
- Pelvic Tilt (PT): The angle formed by a vertical reference line and the line from the sacral plate's midpoint to the femoral heads' center.
- Lordosis distribution index (LDI) determines the magnitude of L4S1 lordosis relative to the total lordosis [35] and was calculated as $LDI = \frac{100 \times (L4\text{–}S1\ lordosis)}{(L1\text{–}S1\ lordosis)}$.

Model instrumentation

The instrumentation (including polyaxial screws and rods) was designed in SolidWorks (Dassault Systèmes SolidWorks Corporation, Waltham, MA, USA). A 4-rod configuration was used for each PSO model (2 primary rods + 2 *in-line* satellite rods). All models included instrumentation from T11 to the pelvis (Fig. 1). Pelvic fixation with traditional iliac screws were connected to the primary rods via an iliac connector. The T11 and T10 segments were selected as the upper instrumented vertebral body (UIV) and upper instrumented vertebral body +1 (UIV+), respectively. All pedicles starting from T11 to the pelvis were instrumented bilaterally with titanium alloy polyaxial screws.

Screws were modeled in 2-parts (tulip + shaft) and connected with a ball and socket joint. The size and length of the pedicle screws for each model were selected under the guidance of the spine surgeons (Table 2). Shorter length pedicle screws were inserted in the vertebra adjacent to the osteotomy site to provide enough room for long rods to bypass the PSO site while short rods fixing the PSO. 8.5×80 mm iliac screws were utilized (Table 2). Two primary rods were inserted from T11 to ilium, bypassing the levels adjacent to the PSO. The adjacent levels to the osteotomy site were then instrumented via 2 *in-line* recessed PSO satellite rods. All models included 5.5 mm Cobalt-Chromium primary and satellite rods.

To simulate polyaxial screws, 2 reference points were defined on the screw shaft and the tulip head, and the corresponding nodes were coupled to each reference point separately. Then a "Join and Cardan" connector was assigned between the shaft and tulip, which constrained the 2 components in U1, U2, and U3 motions and allowed for a relative rotation between these components (UR1, UR2, and UR3). Moreover, a surface-to-surface interaction was defined between the tulip and shaft (friction=0.4). Primary and satellite rods were tied to the tulip in all models.

Loading and boundary conditions

Loading was applied in 2 steps. In step 1, 300 N was applied to the thoracic spine, 400 N to the lumbar spine, and 400 N to the sacrum using the follower load technique [32,33]. In step 2, pure moments of 7.5 Nm were applied to the top endplate of the T10 vertebral body in all 3 anatomical directions. During the simulation, the acetabular surfaces of the pelvis were fixed in all degrees of freedom.

Data analysis

For each model, the spinopelvic parameters such as L1-S1 lordosis (LL), L4-S1 lordosis, sacral slope (SS), pelvic incidence (PI), and pelvic tilt (PT) were captured and compared with the intact alignment. Moreover, the LDI was calculated for each model and compared.

The T10-S1 and T10-T11 ranges of motion (ROM), along with both left and right sacroiliac joint ROMs (SIJ) within all instrumented PSO models, in flexion, extension, lateral bending, and rotation, were calculated. The SIJ ROM for each side was calculated using the difference between the angular displacements at the sacrum and ilium of the corresponding side. Furthermore, the maximum stress magnitude and location on the rods and PSO forces were recorded and compared. The maximum von Mises

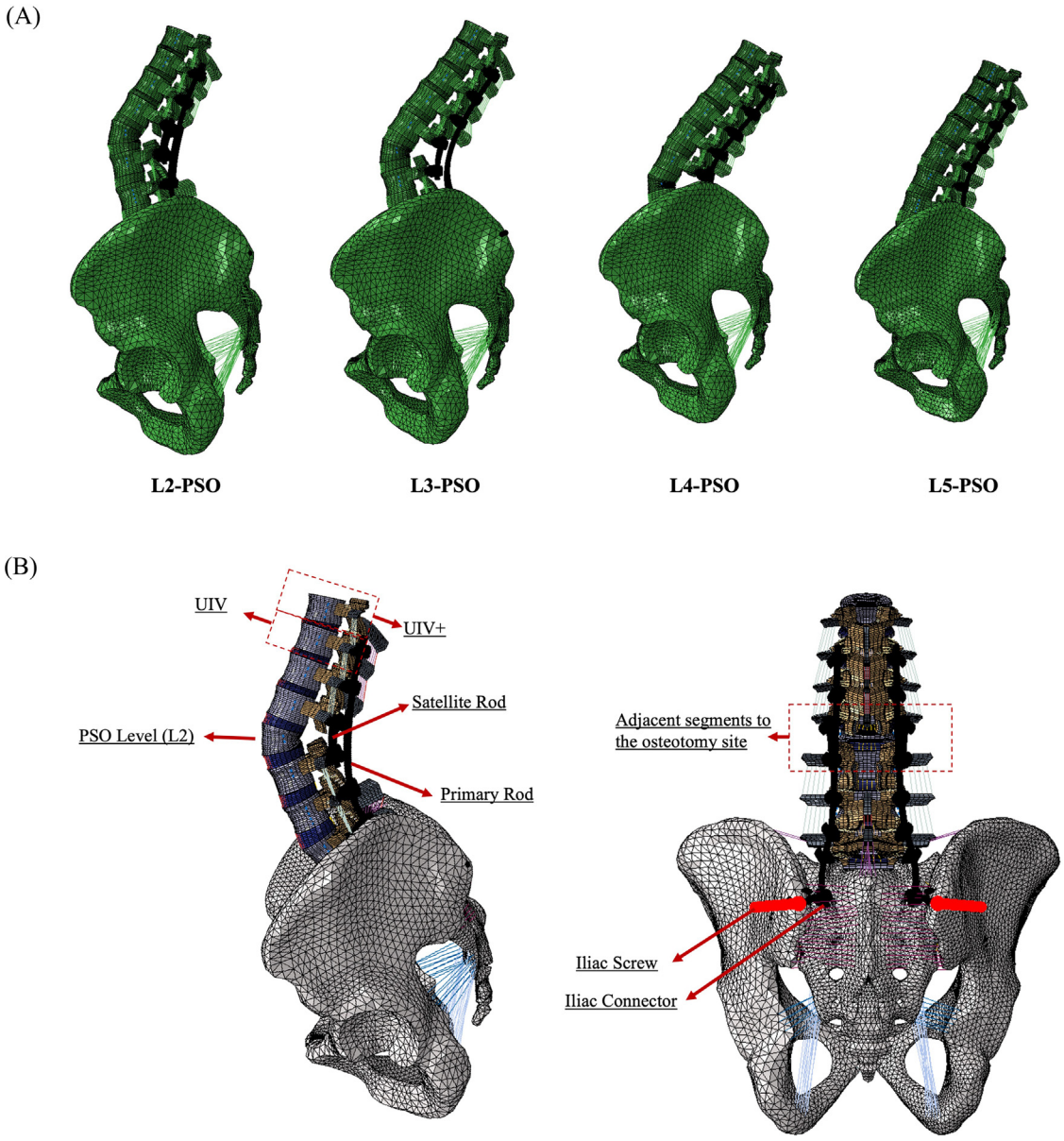

Fig. 1. (A) Lateral view of the developed spinopelvic Finite Element models integrated with a 30° PSO at the L2, L3, L4 and L5 segments accompanied with a 4-rod configuration. Each model was instrumented with (B) two primary rods + 2 *in-line* recessed PSO satellite rods spanning the osteotomy site. All models included instrumentation starting from T11, which was extended to the pelvis. Traditional iliac screws were used as a pelvic fixation, which were connected to the primary rods via iliac connectors. The T11 and T10 segments were selected as the upper instrumented vertebral body (UIV) and upper instrumented vertebral body +1 (UIV+), respectively.

stresses on the anterior parts of T10 (UIV +) and T11 (UIV) vertebral bodies and the T10–T11 intervertebral discs were recorded and evaluated in all models. Given that L3-PSOs are commonly performed, the percentage differences in the aforementioned parameters were compared to this model.

Results

Model validation

The L3- and L4-PSO models were validated to ensure that this model can predict previous experimental and biomechanical outcomes [36–38]. However, due to the lack of available *in-vitro* studies on PSOs at L2 and L5, we were not able to validate these models.

L3-PSO model validation

For the validation of this instrumented PSO model, the range of motion predictions for the L2-L4 instrumented models were compared to the experimental data Hallager et al [39]. Different instrumentation techniques were used for this purpose including 2 rod and 4 rod techniques with different material properties for the rods (Titanium and CoCr rods).

Table 2
Screw dimensions used in each model (diameter × length) (mm)

	PSO-L2	PSO-L3	PSO-L4	PSO-L5
T11	5.5×40	5.5×40	5.5×40	5.5×40
T12	5.5×40	5.5×40	5.5×40	5.5×40
L1	**6.5×40**	6.5×40	6.5×40	6.5×40
L2	[redacted]	**6.5×40**	6.5×40	6.5×40
L3	**6.5×40**	[redacted]	**6.5×40**	6.5×45
L4	6.5×45	**6.5×40**	[redacted]	**6.5×45**
L5	6.5×45	6.5×45	**6.5×40**	[redacted]
S1	7.5×50	7.5×50	7.5×50	**7.5×45**
Ilium	8.5×80	8.5×80	8.5×80	8.5×80
Vertebrae secured to satellite rods	L1 and L3	L2 and L4	L3 and L5	L4 and S1

Screw dimension for each model was selected under the guidance of the spine surgeons. Adjacent to the osteotomy site, screw with a shorter shaft were inserted. The iliac screws were sized 8.5 × 80 mm.

The FE model predictions for all motions (flexion, extension, lateral bending, and axial-rotation) as well as the normalized strains fell within the standard deviation (Fig. 2), validating the L3-PSO model.

L4-PSO model validation

For the validation of this instrumented PSO model, the range of motion predictions in the T12-S1 instrumented model were compared to the experimental data of La Barbera et al [36]. The FE models predictions for all motions fell within the standard deviation (Fig. 3), validating the L4-PSO model.

Effect of PSO level on spinopelvic parameters

Performing the osteotomy at the L4 and L5 vertebra led to the greatest lumbar lordosis corrections. Compared to the intact alignment (LL=49°, Fig. 4), lumbar lordosis increased by 48%, 45%, 59%, and 56% in the L2-, L3-, L4- and L5-PSO models, respectively. Compared with the intact model, L4-S1 lordosis increased by 93%, 101%, in L4 and L5 PSOs while reduced by 13% and 35% in the L2 and L3 PSOs (Fig. 4).

Performing an osteotomy increased the sacral slope (SS) by 25%, 15%, and 11%, in L2 L3, and L4 PSOs, respectively. The pelvic incidence (PI) did not change as a result of lumbar osteotomy while pelvic tilt reduced by 76%, 53%, and 45% in L2, L3, and L4 PSOs. The L5 PSO showed similar sacral slope and pelvic tilt as the intact alignment. Compared to the intact model LDI decreased in the L2 and L3 PSOs (37% and 28%) while increased in the L4 and L5 PSOs (76% and 81%), compared to the intact model (63%).

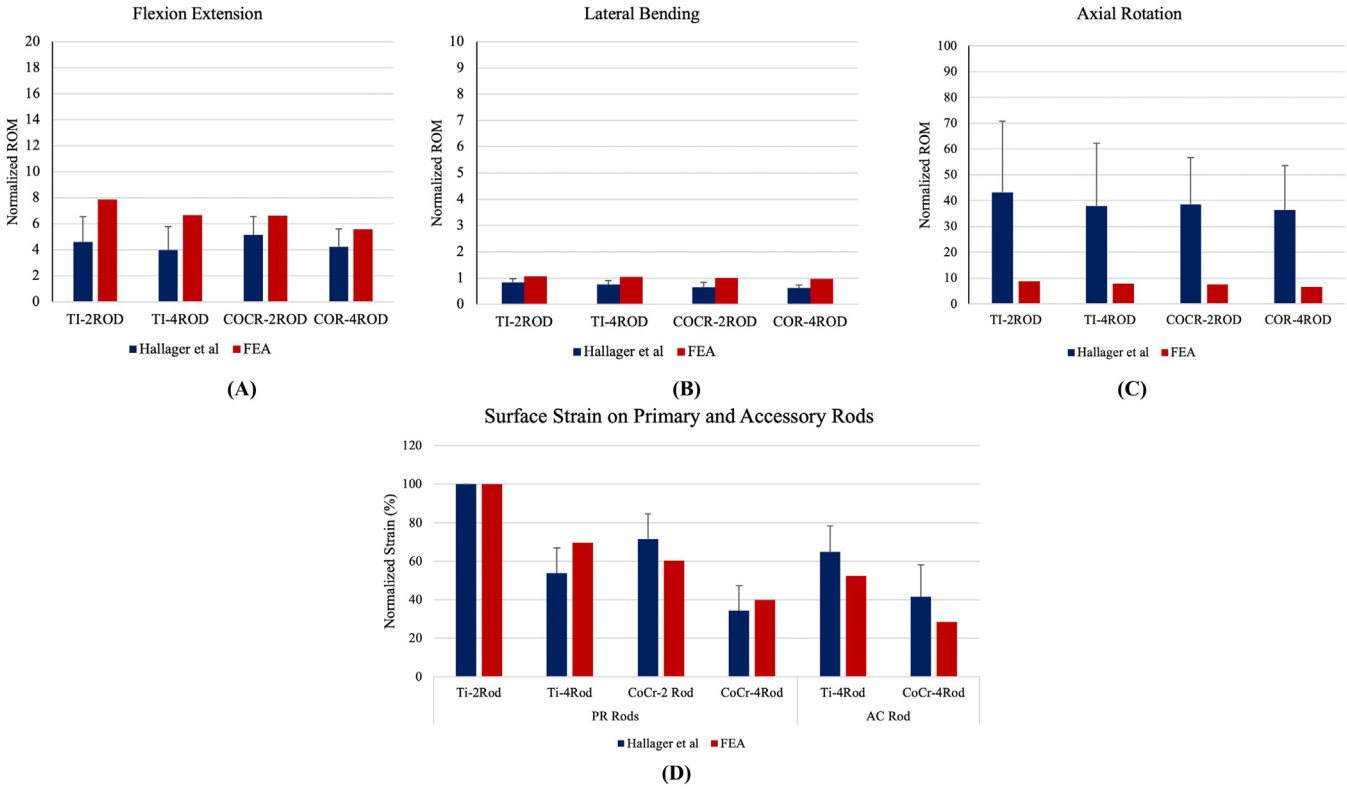

Fig. 2. Validation of the L3-PSO model instrumented with 2 and 4 (Ti and CoCr) rods with the *in-vitro* analysis of Halleger et al. [39]. The FE model predictions for all L3-PSO in all motions fell within the standard deviation. The FE predictions for the strains on primary and accessory rods of the L3-PSO model fell within the standard deviation of the *in vitro* analysis [39].

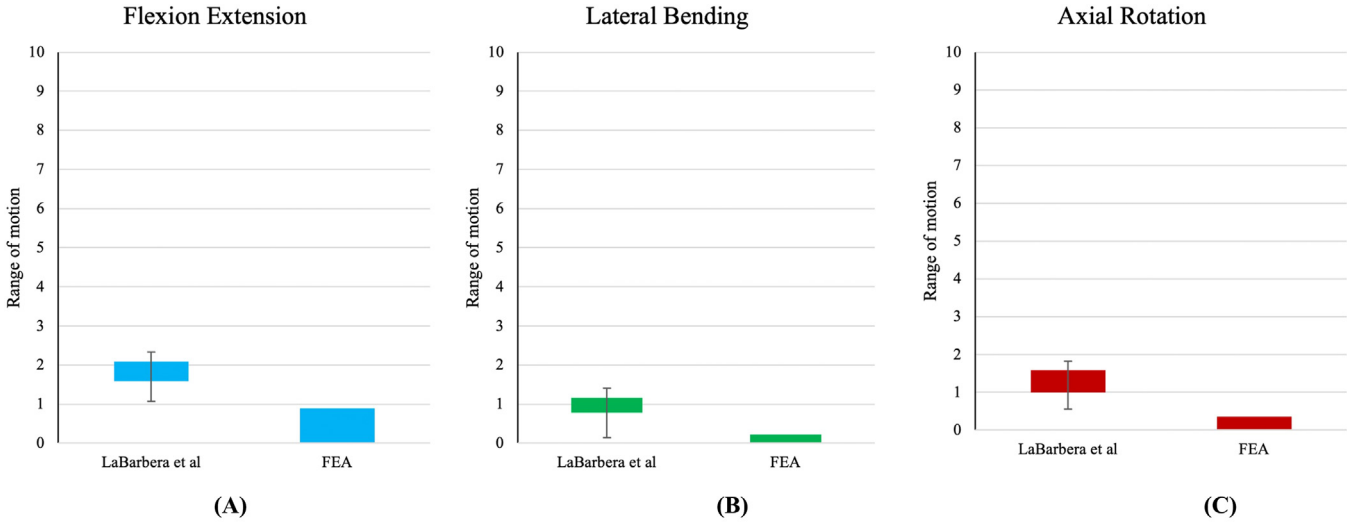

Fig. 3. Validation of the L4-PSO model instrumented with two rods with the *in-vitro* analysis of La Barbera et al. [36]. The FE model predictions for range of motion fell within the standard deviation.

T10-S1 range of motion (global ROM)

The L3 PSO showed the highest global ROM in extension and axial rotation. Compared to this model, L2, L4, and L5 showed 19%, 22%, and 20% lower ROM in extension, respectively. All models showed approximately similar ROM in flexion (differences below 2%). Compared to the L3 PSO, L4 PSO increased ROM in lateral bending (by up to 7%) while L5 PSO reduced the lateral bending ROM to the same extent. Compared to the L3 PSO, the L2, L4, and L5 PSOs reduced ROM in axial rotation by up to 32%, 34%, and 34%, respectively (Fig. 5).

Sacroiliac joint range of motion (SIJ ROM)

All models showed a small range of motion at the sacroiliac joint. The left and right SIJ ROM were approximately similar in each model.

Compared to the L3-PSO, L2-PSO model showed up to 22% and 24% lower ROM in flexion and extension while up to 97% higher ROM in lateral bending and up to 144% higher ROM in axial rotation.

Similar pattern was observed in the L4-PSO model. Compared to the L3-PSO model, ROM decreased in flexion and extension (by up to 24%) while increased in lateral

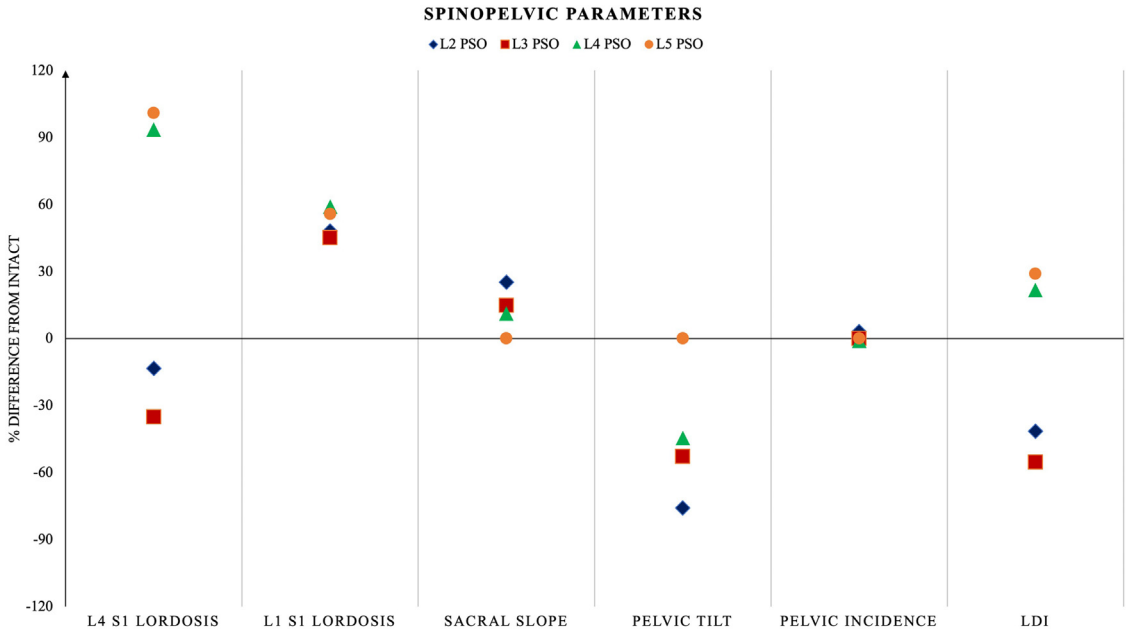

Fig. 4. The percentage difference of spinopelvic parameters of the PSO models with respect to the intact alignment. Compared to the intact alignment: LL increased by 48%, 45%, 59%, and 56% in the L2-, L3-, L4-, and L5-PSO models; SS increased by 25%, 15%, and 11% while PT decreased by 76%, 53%, and 45% in L2-, L3-, and L4-PSOs (SS and PT approximated intact model in L5-PSO); Lumbar osteotomy did not affect the PI.

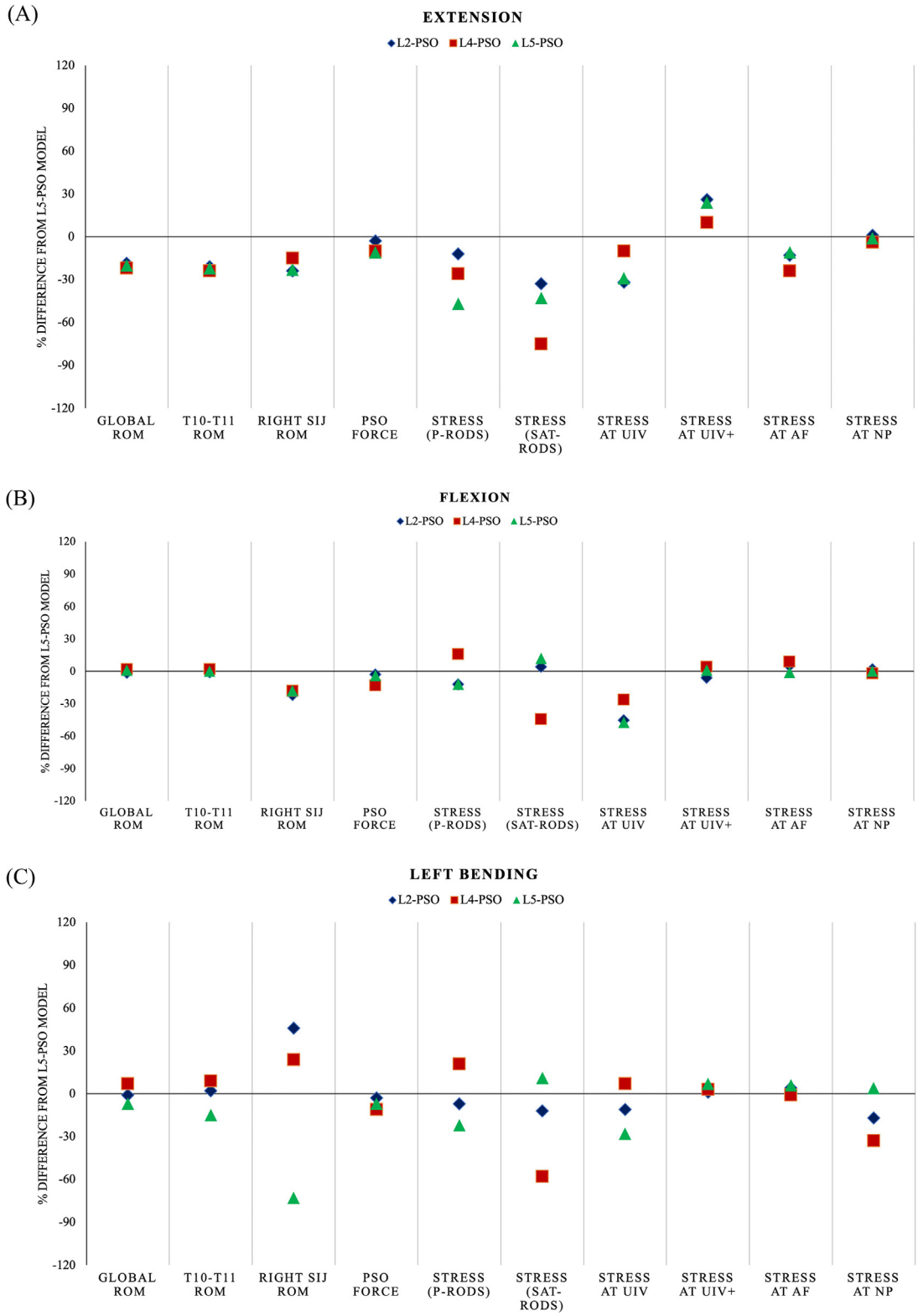

Fig. 5. The percentage difference of the L2-, L4-, and L5-PSOs with respect to the L3-PSO model in (A) extension, (B) flexion, (C) left bending, (D) right bending, (E) left axial rotation, and (F) right axial rotation.

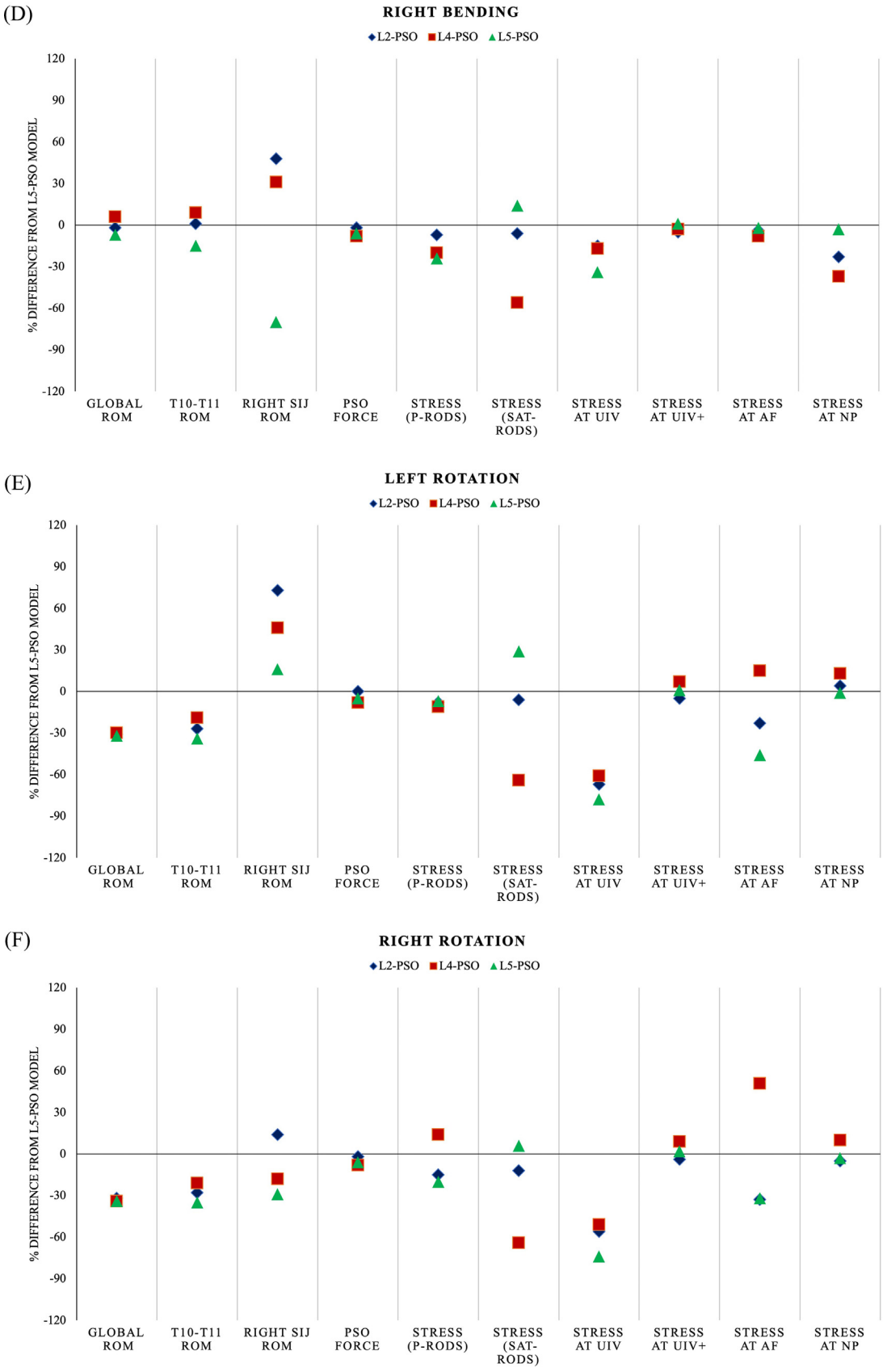

Fig. 5. Continued

bending and axial rotation (by up to 67% and 182% in lateral bending and left rotation). Following an L4-PSO, right SIJ ROM was reduced by 18%, compared with the L3-PSO model.

Amongst all, the L5-PSO model showed the least ROM at the SIJ. Compared to the L3-PSO model, performing osteotomy at L5 reduced the ROM at SIJ by up to 19% in flexion, 23% in extension, and up to 73% in lateral bending. Following L5-PSO, SIJ Rom was increased by up to 47% in left rotation while was reduced by 29% in right rotation.

Adjacent segment range of motion (T10-T11 ROM)

Compared to the L3-PSO model, the T10-T11 ROMs reduced by 21% in extension and up to 28% in axial rotation in L2-PSO model. In this model, the T10-T11 ROM did not change significantly in lateral bending (within 5% difference, Fig. 5).

Compared to L3-PSO model, performing osteotomy at L4 increased the T10-T11 ROM in lateral bending by 9% while reduced the extension and axial rotation by 24% and up to 21%, respectively (Fig. 5).

The L5-PSO showed the least T10-T11 ROM. Compared to L3-PSO, 22%, up to 15% and up to 35% lesser ROM was observed in this model in extension, lateral bending, and axial rotation, respectively (Fig. 5).

All models showed approximately similar ROM in flexion as the L3-PSO model (within 5% difference, Fig. 5).

von mises stresses on UIV, UIV±1 and disc

The least stresses at UIV were observed in the L5-PSO model. The L2-PSO and L5-PSO models showed 11%-67% and 28%-78% lesser von Mises stresses than the L3-PSO model.

Compared to the L3-PSO, the L4-PSO model showed lower stresses in all ROMs (up to 61%) except left bending. Under left bending this model increased the von Mises stresses slightly (by 7%) compared to the L3-PSO.

In all models, higher von Mises stresses were observed at the T10 vertebrae (UIV+) compared to the UIV (T11) (Fig. 5). Compared to the L3-PSO, L2, L4, and L5-PSOs showed 26%, 10%, and 24% higher stresses at UIV+ in extension, respectively. In flexion, L2-PSO reduced the stresses at UIV+, while L4 and L5-PSOs showed approximately similar stresses compared to the L3-PSO model (within 5% difference).

In lateral bending, all models showed approximately similar stresses at UIV+ compared to the L3-PSO model. Under axial rotation, L4-PSO increased the stresses at UIV+ by up to 9% while all other models showed approximately similar stresses as the L3-PSO model (within 5% difference).

Compared to L3-PSO, the L2-PSO model, reduced the stresses at T10-T11 annulus fibrosus (AF) by 13% in extension and up to 33% in axial rotation. However, in flexion and lateral bending, this model showed approximately similar AF stresses as the L3-PSO.

Compared to the L3-PSO, the L4-PSO showed 24% and up to 8% lesser stresses in extension, and lateral bending, respectively. However, this model showed 9% and up to 51% higher AF stresses than the L3-PSO, in flexion and axial rotation, respectively.

Compared to the L3-PSO, the L5-PSO model showed 11%, and up to 46% lesser AF stresses in extension and axial rotation, respectively. Following L5-PSO, AF stresses were approximately similar to the L3-PSO model.

FE predictions showed approximately similar T10-T11intradiscal pressure under flexion and extension in all models (within 5% difference). However, the L2-and L4-PSO models reduced the pressure by up to 23% and 37% in lateral bending, compared with the L3-PSO model. In axial rotation, the L2-PSO model showed up to 13% higher intradiscal pressure, while the percentage difference was not significant in the other 2 models compared to the L3-PSO.The L5-PSO model showed similar intradiscal pressure as the L3-PSO model in all motions (Fig. 5).

PSO force

The maximum PSO force was observed in flexion for all models (Table 3). The L3-PSO model showed the maximum force across the osteotomy site. Compared to this model, the L2-PSO showed approximately similar PSO force with the percentage difference within 5%. However, the L4-PSO and L5-PSO models showed up to 13% and 11% lesser PSO force than the L3-PSO model (Table 3).

Stresses on primary and satellite rods

Compared to the L3-PSO, the L2-PSO model showed up to 15% lower stresses on primary rods. The L4-PSO reduced the stresses on primary rods by 26% in extension, 20% in right bending and 11% in left rotation, compared to the L3-PSO model. However, this model increased the stresses by 16%, 21%, and 14% in flexion, left bending, and right rotation, respectively.

Compared to the L3-PSO model, the L5-PSO showed up to 47% lesser stresses on primary rods.

The L3-PSO model showed the highest stresses on satellite rods in all motions (Fig. 6). Compared to this model,

Table 3
Force across the osteotomy site in models with PSOs at L2, L3, L4, and L5 vertebral bodies

	L2-PSO	L3-PSO	L4-PSO	L5-PSO
Extension	249.2	256	231.0	228.8
Flexion	344.7	354.2	309.0	341.1
Left Bending	292.1	301.4	269.7	279.8
Right Bending	292.7	300.2	275.0	281.6
Left Rotation	291.3	292	268.3	277.7
Right Rotation	290.3	295.4	270.9	278.1

In each model the highest PSO force was obtained in flexion. The L2- and L3-PSO models showed the maximum PSO force.

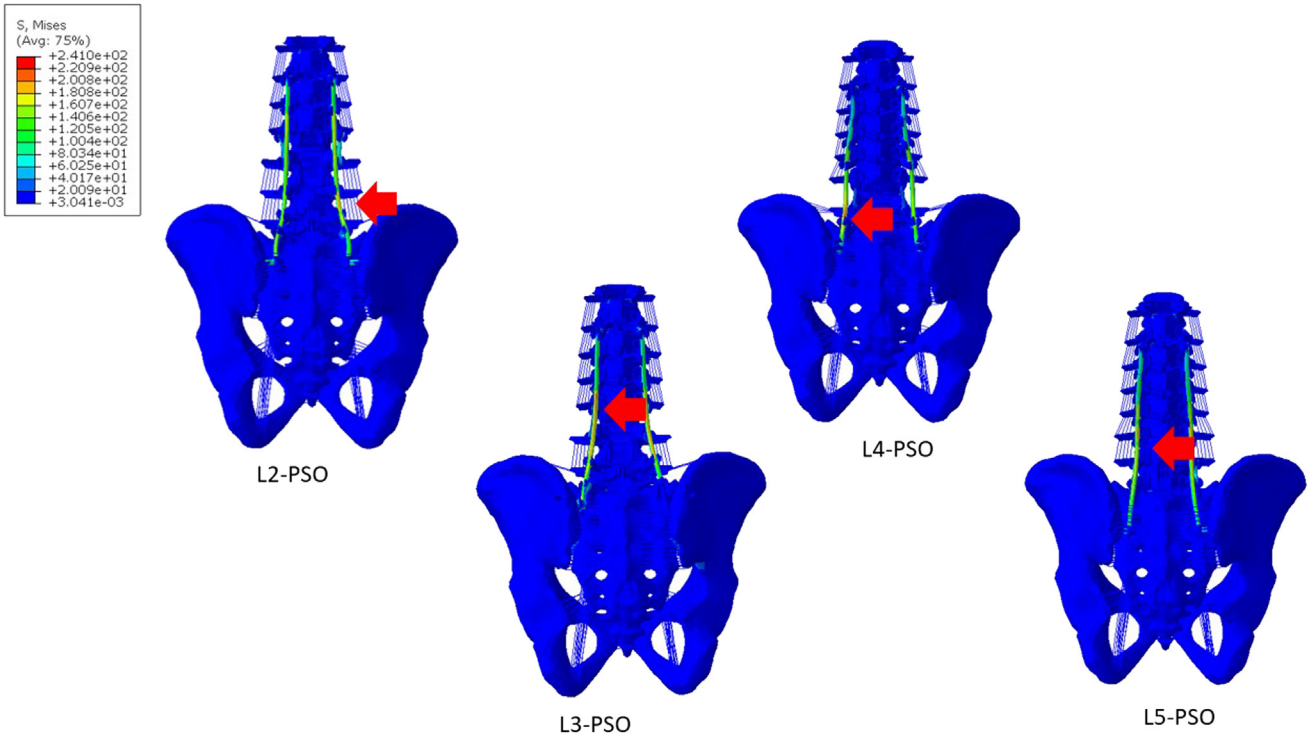

Fig. 6. Stress contour in models with L2, L3, L4, and L5-PSOs. The maximum stress location is shown by a red arrow.

the L2-, L4-, and L5-PSO models showed up to 33%, 75%, and 43% lesser stresses on satellite rods, respectively. Each model demonstrated different critical stress locations, which was secondary to the difference in the rod contour in each model.

Discussion

PSO is a powerful surgical technique often utilized to correct rigid sagittal and coronal spinal deformities. However, PSOs are associated with high rates of complications, including proximal junctional kyphosis, rod / implant failure, and pseudarthrosis [3-12]. Thus, PSOs remain challenging, and it is essential to understand the global biomechanics, rod and proximal junctional stresses, to reduce the risk of postoperative complications that can often require revision surgery.

There are key bony, neurologic, and vascular anatomical considerations for selecting the osteotomy level. Clinically, a patient's individual spinal deformity usually dictates where corrective osteotomies are performed. PSOs are often performed at the apex of the spinal deformity, or the caudal lumbar vertebra (L3-S1) [40]. To optimize sagittal realignment and pelvic parameters more caudal PSOs (L3, L4) are often utilized. The proximity of the more sensitive L5 nerve roots may influence the selection of a L3-PSO over a L4-PSO [40]. Data on more distal L5- and sacral PSOs is limited and may be secondary to the challenges associated with these osteotomies. [41,42] The deeper location of the L5 and S1 vertebra within the pelvis, proximity of the L5 nerve root and anterior vasculature to the osteotomy, and limited distal fixation points may increase the risk of peri- and postoperative complications. [43] Recent clinical studies have suggested that using distal lumbar (L4, L5) and sacral PSOs can optimize lumbar lordosis, sagittal realignment, and pelvic parameters, decreasing the risk of PJK [2,41,42,44-48]. More distal PSOs (L4, L5, and S1) have the ability for greater sagittal plane realignment and improvement of pelvic parameters but may increase the risk of pre- and postoperative complications and warrant further investigation.

We hypothesized that the location of the PSO can alter spinal alignment, and local and global stresses, which can affect the surgical outcomes. Hence, this study attempts to investigate the effect of PSO level on the spine's global (T10-S1), proximal junction (T10-T11), and distal sacroiliac joint (SIJ) ROMs, stresses on the posterior instrumentation, load sharing with the anterior column, and proximal junctional stresses (UIV, UIV+1, and discs).

Given the fact that the L3-PSO is considered the most common osteotomy level, we compared different parameters across each motion with the FE predictions of this L3-PSO model (Fig. 5). Compared with a L3-PSO, the data demonstrates that performing an osteotomy at the L5 segment provided the greatest rigidity, and consequently the least global ROM. This can be explained by the fact that satellite rods in a L5-PSO were attached to L4 and S1, resulting in 5 cranial segments that were anchored to the primary rods (T11, T12, L1, L2, and L3). However, in the models with cranial PSOs, such as a L3-PSO, the number

of cranial vertebral segments fixed to the primary rods were reduced. Thus, the L5-PSO model demonstrated greater rigidity compared to the L3-PSO model. The L2- and L4-PSO models showed similar percentage differences of global ROM from the L3-PSO model (Fig. 5).

Although a 30° correction was uniformly performed in each model, performing an osteotomy at different vertebral levels changed the alignment of the spine and consequently affected biomechanics. Previous studies reveal two-thirds of the total lumbar lordosis is obtained at the lower lumbar segments [1,30], and performing PSOs at more caudal levels led to greater lordosis correction. Our FE predictions showed that the L4 and L5-PSO models led to the highest L1S1 lordosis corrections. Compared to the intact model, lumbar lordosis increased by 48%, 45%, 59%, and 56% in the L2-, L3-, L4- and L5-PSO models, respectively. Bourghli A, et al reported similar corresponding pattern in lumbar lordosis following L4- and L5-PSOs [2]. Relative to the preoperative values, the L4-S1 lordosis was increased following L4 and L5-PSOs while reduced in L2 and L3-PSOs. This reduction was previously observed in the study of Pizones et al [49].

Additionally, PSOs at L2-, L3-, L4-, and L5 changed the sacral slope by 25%, 15%, 11%, and 0%, respectively.

In agreement with previous data, pelvic incidence did not change as a result of lumbar osteotomy while pelvic tilt was also affected by PSO level [50].

As indicated by Roussouly et al [1], lumbar lordosis can be divided into the lower and upper arcs (the upper arc extends from the apex to the inflexion point, while the lower arc extends from S1 to the apex). We observed that performing osteotomies at caudal segments lead to a larger lower arc (L4S1 lordosis). Moreover, the lordosis distribution index (LDI) calculated in each model showed that for intact, L4-, and L5-PSOs, LDI ranged from 63 to 81, while the L2-, and L3-PSOs <50. Previous data reveals a greater risk for revision surgery in cases where the LDI <50 [35]. Thus, more caudal PSOs (L4 and L5) recreates a more anatomic lordosis distribution compared to more cranial PSOs (L2 and L3).

Our FE data revealed that the least SIJ ROM was observed in 2 models, the L5-PSO under flexion, extension, and lateral bending, and the L3-PSO under axial rotation. Ushirozako et al [51] reported screw loosening in 25% of L5-PSO cases, which was significantly higher than patients undergoing an L4-PSO (8%) and L1-L3 PSOs (15%). The stiffer L5-PSO constructs may not allow for micromotion, thereby increasing the risk of screw loosening. The utilization of bilateral iliac screw fixation may mitigate the risk of screw loosening in L5-PSOs [51].

The development of proximal junctional kyphosis (PJK) is a common postoperative complication in adult spinal deformity (ASD) patients [48,52]. In patients with long instrumented segmental fusions, the increased stresses at the proximal junction, can increase the risk of PJK, which may lead to proximal junctional failure (PJF) and resultant revision surgery. Previous data demonstrates that larger lumbar lordosis corrections can increase the risk of PJK [50], while proper rod contouring and UIV selection can be beneficial to mitigate the risk of PJK [53]. Our FE data, reveals that the L3- and L4-PSOs demonstrates higher stresses at UIV and UIV+ compared to the L5-PSO model. Ushirozako et al [51] demonstrated clinical results validating our FE data, in that patients undergoing an L5-PSO resulted in the lowest incidence of PJF (8.3%), compared to L4- (16%), and L1-, L2-, and L3-PSOs (20%).

Additionally, the low rate of PJK in patients with an L5-PSO could also be explained by the lowest T10-T11 ROM compared to other PSO models (Fig. 5). Compared to the L3-PSO, the L2- and L4-PSOs demonstrated an increased T10-T11 ROM under lateral bending. Reducing the ROM, particularly in flexion, can decrease the load and stresses applied to the vertebral bodies, thereby reducing the risk of PJK and PJF [2,54]. Biomechanically, caudal PSOs may be more beneficial, but bony, soft tissue, and technical considerations may limit their utility.

Rod fracture is another common complication associated with PSOs, which has been reported as high as 22% [55]. Our data reveals that the L5-PSO model demonstrates the least von Mises stresses on the primary rods in all motions (Fig. 5). These results were consistent with the retrospective study of Ushirozako et al [51], which showed lower incidences of rod fracture in patients with L5-PSOs, compared to L4- and L1−L3 (25% vs 56% and 30%, respectively).

The FE data for the L2- and L3-PSO models demonstrated the highest force across the osteotomy site, while the L4- and L5-PSOs revealed the least force. The decreased load applied to the anterior vertebral body in L5-PSOs, along with a reduction in distal construct length as compared to L1−L4 PSOs can increase the risk of pseudarthrosis [49]. However, further clinical analysis is essential to validate these data.

The results of this study should be considered in the context of its limitations. These include using generic implants and neglecting the residual stresses produced as a result of rod contouring and screw/rod tightening.

Moreover, due to the lack of cadaveric validation data for L2 and L5 and given L5′s unique structural differences compared to other spinal levels, PSOs at this level might exhibit the most significant deviations from biomechanical/cadaver models. Thus, the results of this study should be considered within their limitations, and further clinical investigations are necessary to fully understand the complex biomechanical environment produced by caudal osteotomies.

All PSO models were reconstructed using an intact alignment, hence relatively large LL and SS were observed in all models. The spinopelvic parameters from the current study represent the values right after the surgery and it does not consider the effect of fusion or dynamic loading at the sacroiliac joint. The estimated 30° correction is an idealized maximum value and may not be clinically achievable due

to the large amount of bone resected. This represents a worst-case scenario, so clinical results may differ from the FEA outcomes.

Moreover, fixing the acetabulum surfaces in all degrees of freedom affects the range of motion at the sacroiliac joint due to its kinematics. Future studies should be focused on developing a spinopelvic model with hip joint and investigate how shear forces at the sacroiliac joints affect the spine's biomechanics following a lumbar PSO.

Conclusion

Our FE data indicates that the L5-PSO resulted in the greatest lumbar lordosis, while showing the least global, SIJ, and proximal junction (T10-T11) ROMs and stresses on the primary rods, suggesting potential mechanical benefits in reducing the risk of rod breakage. However, L4- and L5-PSOs result in the least force across the osteotomy site, which may increase the risk of pseudarthrosis. Additionally, the technical considerations; the bony, L5 nerve, and anterior vascular anatomy; and the limited distal fixation points should all be considered when a caudal PSO is being contemplated. These findings provide biomechanical insights that may inform surgical planning, though further clinical investigation is essential to determine the optimal PSO level and validate these results.

Declaration of competing interest

One or more of the authors declare financial or professional relationships on ICMJE-TSJ disclosure forms.

CRediT authorship contribution statement

Niloufar Shekouhi: Writing – review & editing, Writing – original draft, Validation, Methodology, Formal analysis, Data curation, Conceptualization. **Sudharshan Tripathi:** Writing – review & editing, Writing – original draft, Validation, Methodology, Formal analysis, Data curation, Conceptualization. **Alekos Theologis:** Writing – review & editing, Supervision, Formal analysis, Conceptualization. **Muzammil Mumtaz:** Formal analysis, Data curation. **Hassan Serhan:** Writing – review & editing. **Robert McGuire:** Writing – review & editing, Writing – original draft, Supervision, Formal analysis, Conceptualization. **Vijay K. Goel:** Investigation, Funding acquisition, Formal analysis, Conceptualization. **Joseph M. Zavatsky:** Writing – review & editing, Writing – original draft, Supervision, Formal analysis, Conceptualization.

Acknowledgments

The work was supported in part by NSF Industry/University Cooperative Research Center at The University of California at San Francisco, San Francisco, CA, The University of Toledo, Toledo, OH, and The Ohio State University, Columbus, OH (www.nsfcdmi.org).

References

[1] Roussouly P, Pinheiro-Franco JL. Sagittal parameters of the spine: Biomechanical approach. Eur Spine J 2011;20(5):578–85.
[2] Bourghli A, Boissiere L, Chevillotte T, et al. Radiographic outcomes and complications after L4 or L5 pedicle subtraction osteotomy for fixed sagittal malalignment in 102 adult spinal deformity patients with a minimum 2-year follow-up. Eur Spine J 2021:1–8.
[3] La Barbera L, Wilke HJ, Ruspi ML, et al. Load-sharing biomechanics of lumbar fixation and fusion with pedicle subtraction osteotomy. Sci Rep 2021;11(1):3595.
[4] Smith JS, Shaffrey CI, Klineberg E, et al. Complication rates associated with 3-column osteotomy in 82 adult spinal deformity patients: retrospective review of a prospectively collected multicenter consecutive series with 2-year follow-up. J Neurosurg 2017;27(4):444–57.
[5] Gupta S, Eksi MS, Ames CP, et al. A novel 4-rod technique offers potential to reduce rod breakage and pseudarthrosis in pedicle subtraction osteotomies for adult spinal deformity correction. Oper Neurosurg (Hagerstown) 2018;14(4):449–56.
[6] Luca A, Lovi A, Galbusera F, Brayda-Bruno M. Revision surgery after PSO failure with rod breakage: A comparison of different techniques. Eur Spine J 2014;23(6):610–5.
[7] Hyun SJ, Lenke LG, Kim YC, Koester LA, Blanke KM. Comparison of standard 2-rod constructs to multiple-rod constructs for fixation across 3-column spinal osteotomies. Spine (Phila Pa 1976) 2014;39 (22):1899–904.
[8] Smith JS, Shaffrey E, Klineberg E, et al. Prospective multicenter assessment of risk factors for rod fracture following surgery for adult spinal deformity. J Neurosurg 2014;21(6):994–1003.
[9] Smith JS, Shaffrey CI, Ames CP, et al. Assessment of symptomatic rod fracture after posterior instrumented fusion for adult spinal deformity. Neurosurgery 2012;71(4):862–8.
[10] Kim YJ, Bridwell KH, Lenke LG, Cheh G, Baldus C. Results of lumbar pedicle subtraction osteotomies for fixed sagittal imbalance: A minimum 5-year follow-up study. Spine 2007;32(20):2189–97.
[11] Kim YC, Kim KT, Kim CK, et al. Outcomes of non-operative management for pseudarthrosis after pedicle subtraction osteotomies at minimum 5 years follow-up. J Korean Neurosurg Soc 2019;62 (5):567–76.
[12] Bridwell KH, Lewis SJ, Lenke LG, Baldus C, Blanke K. Pedicle subtraction osteotomy for the treatment of fixed sagittal imbalance. JBJS 2003;85(3):454–63.
[13] Faundez AA, Tsoupras A, Le Huec J-C. Posterior opening wedge osteotomy (POWO) in a patient with thoraco-lumbar proximal junctional failure due to iatrogenic lumbar hyperlordosis. Orthopaed Traumatol 2020:102657.
[14] Lee J, Park Y-S. Proximal junctional kyphosis: Diagnosis, pathogenesis, and treatment. Asian Spine J 2016;10(3):593.
[15] Kim HJ, Iyer S. Proximal junctional kyphosis. JAAOS 2016;24 (5):318–26.
[16] Glattes RC, Bridwell KH, Lenke LG, Kim YJ, Rinella A, Edwards C. Proximal junctional kyphosis in adult spinal deformity following long instrumented posterior spinal fusion: Incidence, outcomes, and risk factor analysis. Spine 2005;30(14):1643–9.
[17] Maruo K, Ha Y, Inoue S, et al. Predictive factors for proximal junctional kyphosis in long fusions to the sacrum in adult spinal deformity. Spine 2013;38(23):E1469–E76.
[18] Kim YJ, Lenke LG, Bridwell KH, et al. Proximal junctional kyphosis in adolescent idiopathic scoliosis after 3 different types of posterior segmental spinal instrumentation and fusions: incidence and risk factor analysis of 410 cases. Spine 2007;32(24):2731–8.
[19] Bridwell KH, Lenke LG, Cho SK, et al. Proximal junctional kyphosis in primary adult deformity surgery: Evaluation of 20 degrees as a critical angle. Neurosurgery 2013;72(6):899–906.
[20] Lowe TG, Kasten MD. An analysis of sagittal curves and balance after Cotrel-Dubousset instrumentation for kyphosis secondary to

Scheuermann's disease. A review of 32 patients. Spine 1994;19 (15):1680–5.
[21] Lee GA, Betz RR, Clements DH, Huss GK. Proximal kyphosis after posterior spinal fusion in patients with idiopathic scoliosis. Spine 1999;24(8):795–9.
[22] Yagi M, Akilah KB, Boachie-Adjei O. Incidence, risk factors and classification of proximal junctional kyphosis: Surgical outcomes review of adult idiopathic scoliosis. Spine 2011;36(1):E60–E8.
[23] Wang J, Zhao Y, Shen B, Wang C, Li M. Risk factor analysis of proximal junctional kyphosis after posterior fusion in patients with idiopathic scoliosis. Injury 2010;41(4):415–20.
[24] Kim YJ, Bridwell KH, Lenke LG, Kim J, Cho SK. Proximal junctional kyphosis in adolescent idiopathic scoliosis following segmental posterior spinal instrumentation and fusion: Minimum 5-year follow-up. Spine 2005;30(18):2045–50.
[25] Kim HJ, Yagi M, Nyugen J, Cunningham ME, Boachie-Adjei O. Combined anterior-posterior surgery is the most important risk factor for developing proximal junctional kyphosis in idiopathic scoliosis. Clin Orthopaed Relat Res 2012;470(6):1633–9.
[26] Mendoza-Lattes S, Ries Z, Gao Y, Weinstein SL. Proximal junctional kyphosis in adult reconstructive spine surgery results from incomplete restoration of the lumbar lordosis relative to the magnitude of the thoracic kyphosis. Iowa Orthop J 2011;31:199.
[27] O'Shaughnessy BA, Bridwell KH, Lenke LG, et al. Does a long-fusion "T3-sacrum" portend a worse outcome than a short-fusion "T10-sacrum" in primary surgery for adult scoliosis? Spine 2012;37 (10):884–90.
[28] Denis F, Sun EC, Winter RB. Incidence and risk factors for proximal and distal junctional kyphosis following surgical treatment for Scheuermann kyphosis: minimum five-year follow-up. Spine 2009;34(20):E729–E34.
[29] Lafage V, Schwab F, Vira S, et al. Does vertebral level of pedicle subtraction osteotomy correlate with degree of spinopelvic parameter correction? Journal of Neurosurgery: Spine 2011;14(2):184–91.
[30] Laouissat F, Sebaaly A, Gehrchen M, Roussouly P. Classification of normal sagittal spine alignment: refounding the Roussouly classification. Eur Spine J 2018;27(8):2002–11.
[31] Yilgor C, Sogunmez N, Yavuz Y, et al. Global alignment and proportion (GAP) score: development and validation of a new method of analyzing spinopelvic alignment to predict mechanical complications after adult spinal deformity surgery. Spine J 2017;17(10):S155–S6.
[32] Seyed Vosoughi A, Joukar A, Kiapour A, et al. Optimal satellite rod constructs to mitigate rod failure following pedicle subtraction osteotomy (PSO): A finite element study. Spine J 2019;19(5):931–41.
[33] Vosoughi AS, Shekouhi N, Joukar A, Zavatsky M, Goel VK, Zavatsky JM. Lumbar disc degeneration affects the risk of rod fracture following PSO; a finite element study. Glob Spine J 2022:21925682221081797.
[34] Imai N, Suzuki H, Nozaki A, Hirano Y, Endo N. Correlation of tilt of the anterior pelvic plane angle with anatomical pelvic tilt and morphological configuration of the acetabulum in patients with developmental dysplasia of the hip: a cross-sectional study. J Orthopaed Surg Res 2019;14(1):1–7.
[35] Bari TJ, Heegaard M, Bech-Azeddine R, Dahl B, Gehrchen M. Lordosis distribution index in short-segment lumbar spine fusion—can ideal lordosis reduce revision surgery and iatrogenic deformity? Neurospine 2021;18(3):543.
[36] La Barbera L, Brayda-Bruno M, Liebsch C, et al. Biomechanical advantages of supplemental accessory and satellite rods with and without interbody cages implantation for the stabilization of pedicle subtraction osteotomy. Eur Spine J 2018;27(9):2357–66.
[37] Ottardi C, Galbusera F, Luca A, et al. Finite element analysis of the lumbar destabilization following pedicle subtraction osteotomy. Med Eng Phys 2016;38(5):506–9.
[38] BdA Pereira, J Godzik, Lehrman JN, et al. Pedicle subtraction osteotomy construct optimization: a cadaveric study of various multirod and interbody configurations. Spine 2022;47(8):640–7.
[39] Hallager DW, Gehrchen M, Dahl B, et al. Use of supplemental short pre-contoured accessory rods and cobalt chrome alloy posterior rods reduces primary rod strain and range of motion across the pedicle subtraction osteotomy level: An in vitro biomechanical study. Spine (Phila Pa 1976) 2016;41(7):E388–95.
[40] Chan AK, Mummaneni PV, Shaffrey CI. Approach selection: Multiple anterior lumbar interbody fusion to recreate lumbar lordosis versus pedicle subtraction osteotomy: when, why, how? Neurosurg Clin 2018;29(3):341–54.
[41] Radcliff KE, Jakoi AM. L5 pedicle subtraction osteotomy for high-grade isthmic spondylolisthesis. Orthopedics 2015;38(4):e347–e51.
[42] Wangdi K, Otsuki B, Fujibayashi S, Tanida S, Masamoto K, Matsuda S. Sagittal imbalance treated with L5 pedicle subtraction osteotomy with short lumbar fusion from L4 to sacrum using four screws into L4 for enhanced fixation two additional vertebral screws: a technical note. Eur Spine J 2019;28(1):121–6.
[43] Yao Z, Zheng G, Zhang Y, et al. Selection of lowest instrumented vertebra for thoracolumbar kyphosis in ankylosing spondylitis. Spine 2016;41(7):591–7.
[44] Funao H, Kebaish FN, Skolasky RL, Kebaish KM. Clinical results and functional outcomes after three-column osteotomy at L5 or the sacrum in adult spinal deformity. Eur Spine J 2020;29(4):821–30.
[45] Alzakri A, Boissière L, Cawley DT, et al. L5 pedicle subtraction osteotomy: Indication, surgical technique and specificities. Eur Spine J 2018;27(3):644–51.
[46] Lee KY, Lee JH, Kang KC, et al. Minimally invasive multilevel lateral lumbar interbody fusion with posterior column osteotomy compared with pedicle subtraction osteotomy for adult spinal deformity. Spine J 2020;20(6):925–33.
[47] Lee KY, Lee JH, Kang KC, et al. Strategy for obtaining solid fusion at L5-S1 in adult spinal deformity: Risk factor analysis for nonunion at L5-S1. J Neurosurg Spine 2020:1–9.
[48] Smith JS, Shaffrey CI, Ames CP, Lenke LG. Treatment of adult thoracolumbar spinal deformity: Past, present, and future: JNSPG 75th Anniversary Invited Review Article. J Neurosurg 2019;30(5):551–67.
[49] Pizones J, Moreno-Manzanaro L, Perez-Grueso FJS, et al. Effect of lumbar pedicle subtraction osteotomy level on lordosis distribution and shape. Eur Spine J 2020;29(6):1388–96.
[50] Lafage R, Obeid I, Liabaud B, et al. Location of correction within the lumbar spine impacts acute adjacent-segment kyphosis. J Neurosurg 2018;30(1):69–77.
[51] Ushirozako H, Hasegawa T, Yamato Y, et al. L5 pedicle subtraction osteotomy maintains good radiological and clinical outcomes in elderly patients with a rigid kyphosis deformity: a more than 2-year follow-up report. Eur Spine J 2020;29(12):3018–27.
[52] Smith JS, Klineberg E, Lafage V, et al. Prospective multicenter assessment of perioperative and minimum 2-year postoperative complication rates associated with adult spinal deformity surgery. J Neurosurg 2016;25(1):1–14.
[53] Lafage R, Line BG, Gupta S, et al. Orientation of the upper-most instrumented segment influences proximal junctional disease following adult spinal deformity surgery. Spine 2017;42(20):1570–7.
[54] Doodkorte RJ, Vercoulen TF, Roth AK, de Bie RA, Willems PC. Instrumentation techniques to prevent proximal junctional kyphosis and proximal junctional failure in adult spinal deformity correction—a systematic review of biomechanical studies. Spine J 2021;21(5):842–54.
[55] Liu H, Wang H, Liu J, Li C, Zhou Y, Xiang L. Biomechanical comparison of posterior intermediate screw fixation techniques with hybrid monoaxial and polyaxial pedicle screws in the treatment of thoracolumbar burst fracture: a finite element study. J Orthopaed Surg Res 2019;14(1):1–8.